

Reduced graphene oxide/porous Si composite as anode for high-performance lithium ion batteries

Hua-Chao Tao · Xue-Lin Yang · Lu-Lu Zhang · Shi-Bing Ni

Received: 29 April 2014 / Revised: 27 July 2014 / Accepted: 28 July 2014 / Published online: 16 August 2014
© Springer-Verlag Berlin Heidelberg 2014

Abstract Reduced graphene oxide/porous Si composite was fabricated through magnesiothermic reduction of mesoporous silica and subsequent dispersing porous Si in the suspension of graphene oxide followed by reduced process. The electrochemical performance of the obtained reduced graphene oxide/porous Si composite was investigated as anode for lithium ion batteries, and it delivers a reversible capacity of about 815 mAh g⁻¹ at a rate of 100 mA g⁻¹ in the voltage range of 0.01–1.5 V after 50 cycles. The excellent electrochemical performance of the composite can be attributed to that of the porous structure of conductive reduced graphene oxide network, and dispersed Si particles can improve electronic conductivity and accommodate the large volume changes.

Keywords Li-ion batteries · Anodes · Electrochemical characterizations · Electrochemical stabilities · Charging/discharging

Introduction

Lithium ion batteries have attracted considerable attention in the various portable electronic devices and electric and hybrid vehicles because of their high energy density and long cycle life. Among various anode materials, silicon is considered as an

ideal anode material for the next-generation lithium ion batteries due to its highest theoretical capacity (4,200 mAh g⁻¹) and satisfactory potentials for lithium ion insertion and extraction (<0.5 V vs. Li/Li⁺) [1]. In addition, silicon is an attractive anode material for lithium ion batteries due to its high abundance and environmental benignity. However, little has been done in utilizing Si as an anode material, mainly due to the large volume changes (~300 %) during lithium ion insertion/extraction process and low electronic conductivity [2]. The large volume changes lead to the fracture and pulverization of electrode materials, which cause rapid capacity fading. Various methods have been adopted to improve the cycling stability of Si-based materials, including decreasing the particles size to nanometer [3–6] and preparation of silicon/carbon composites [7–11].

Among various carbon materials, graphene is a good matrix to host active materials for energy application due to its high electronic conductivity [12], flexibility [13], stability, and large surface area (theoretical value of 2,630 m² g⁻¹) [14]. Graphene [15] and graphene-based materials such as graphene/TiO₂ [16], graphene/Fe₃O₄ [17], graphene/Co₃O₄ [18], graphene/Sn [19], and graphene/SnO₂ [20] have been studied as anode materials for lithium ion batteries. The enhanced electrochemical performance can be due to the improved electronic conductivity, enhanced dispersity of nanoparticles, and the formation of stable solid electrolyte interface (SEI) layer on the electrode surface. Recently, graphene/Si composites have been reported to obtain enhanced electrochemical performance. The graphene/silicon paper exhibits an excellent electrochemical performance due to the good mechanical properties of graphene matrix and improved electronic conductivity of electrode materials [21, 22]. Graphene/silicon powder electrode also demonstrates a high reversible capacity and enhanced cycling stability because graphene-encapsulated silicon composite enhances the compatibility of electrode materials and electrolyte [23].

H.-C. Tao · X.-L. Yang (✉) · L.-L. Zhang · S.-B. Ni
College of Materials and Chemical Engineering, China Three Gorges University, 8 Daxue Road, Yichang, Hubei 443002, China
e-mail: xlyang@ctgu.edu.cn

H.-C. Tao · X.-L. Yang · L.-L. Zhang · S.-B. Ni
Hubei Provincial Collaborative Innovation Center for New Energy Microgrid, China Three Gorges University, Yichang, China

Porous structured materials are of great interest in lithium ion batteries because of large surface area. Porous structure can provide free space for alleviating the structure strain and accommodating the large volume changes, especially Si-based materials. 3D porous Si/C particles have been prepared to obtain excellent cycling performance as anode materials because large porous structures provide empty space to accommodate the volume changes of Si-based materials and release stress during lithium ion insertion process [24]. Macroporous Si/Ag composite also has been prepared to obtain high capacity and good cycling performance because Ag coating layer improves electronic conductivity and porous structure alleviates volumetric stress caused by lithium ion insertion/extraction [25].

Combining the advantages of porous structure and carbon coating, in this study, the reduced graphene oxide/porous Si (RGO/PS) composite has been prepared through a three-step method. The composite exhibits a high reversible capacity of about 815 mAh g⁻¹ after 50 cycles and good cycling stability as anode materials for lithium ion batteries.

Experimental

Preparation of RGO/PS composite

The RGO/PS composite was prepared by a three-step method. Firstly, graphite oxide was synthesized by using a modified Hummers method [26]. The resulting graphite oxide (100 mg) was re-dispersed into deionized water (200 mL) and exfoliated to graphene oxide nanosheets by sonication. Secondly, mesoporous SiO₂ (SBA-15) was prepared according to the literature [27]. The PS particles were obtained by magnesiothermic reduction of SBA-15. SBA-15 (1 g) and magnesium powder (0.5 g) were placed on two close porcelain boats and then sealed with a stainless steel chamber. The sealed chamber was heated at 650 °C for 3 h and then cooled naturally to room temperature. The obtained mixture was washed in 1 mol L⁻¹ HCl solution to remove MgO. Finally, the obtained PS (100 mg) particles were dispersed into a 200-mL graphene oxide nanosheet (0.5 mg mL⁻¹) suspension by sonication. The resulting graphene oxide nanosheets/PS composite was heated at 800 °C for 3 h under Ar atmosphere to obtain the RGO/PS composite.

Structural characterization

The structure was characterized by X-ray diffraction (Rigaku Ultima IV) with Cu K α radiation. The morphologies of graphene oxide nanosheets, SBA-15, PS, and RGO/PS were analyzed by field emission scanning electron microscopy (FE-SEM, JSM-7500 F, JEOL). C, Si, and O maps were collected using the energy dispersive X-ray spectroscopy (EDS, Oxford

X-Max 50) attached to the FE-SEM. The carbon content was determined using thermogravimetric analysis (TGA, Perkin-Elmer 2400II) from 30 to 1,000 °C in air.

Electrochemical characterization

The active materials (PS and RGO/PS composite) were mixed with carbon black and polyvinylidene difluoride (PVDF) at a weight ratio of 80:10:10 for preparing a working electrode. The resulting slurry was uniformly pasted on Cu foil and then dried at 120 °C for 24 h under vacuum. The electrochemical measurements were carried out in 2,032 coin cells with 1 M LiPF₆ in ethylene carbonate/dimethyl carbonate in a volume ratio of 1:1 as the electrolyte and a Li foil as the counter electrode. Coin cells were assembled in an Ar-filled glove box with water and oxygen contents below 1 ppm. The lithium ion insertion and extraction performance was obtained at a rate of 100 mA g⁻¹ in the voltage range of 0.01–1.5 V on a Land CT2100 battery test system. All of the capacities were calculated on the basis of the total weight of composite. Cyclic voltammetry (CV) was carried out using a CHI660C electrochemical workstation (Shanghai Chenhua) at a scan rate of 0.5 mV s⁻¹. Electrochemical impedance spectra (EIS) were measured from 100 kHz to 0.01 Hz with an alternating amplitude of 5 mV by using a CHI660C electrochemical workstation (Shanghai Chenhua).

Results and discussion

The obtained RGO/PS composite was investigated by X-ray diffraction. The XRD patterns of graphite, graphite oxide, SBA-15, PS, and RGO/PS composite were collected as shown in Fig 1. The pristine graphite shows a sharp crystalline peak at 26.5° corresponding to (002) plane. For the graphite oxide,

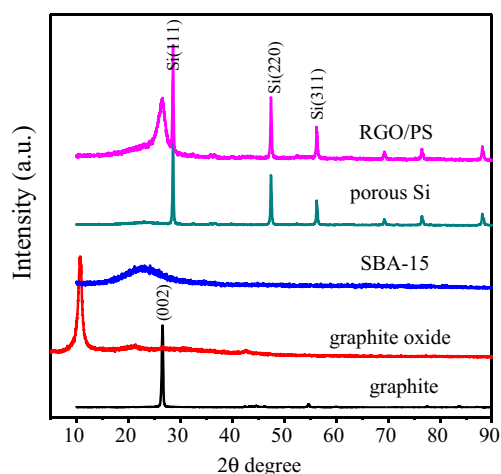


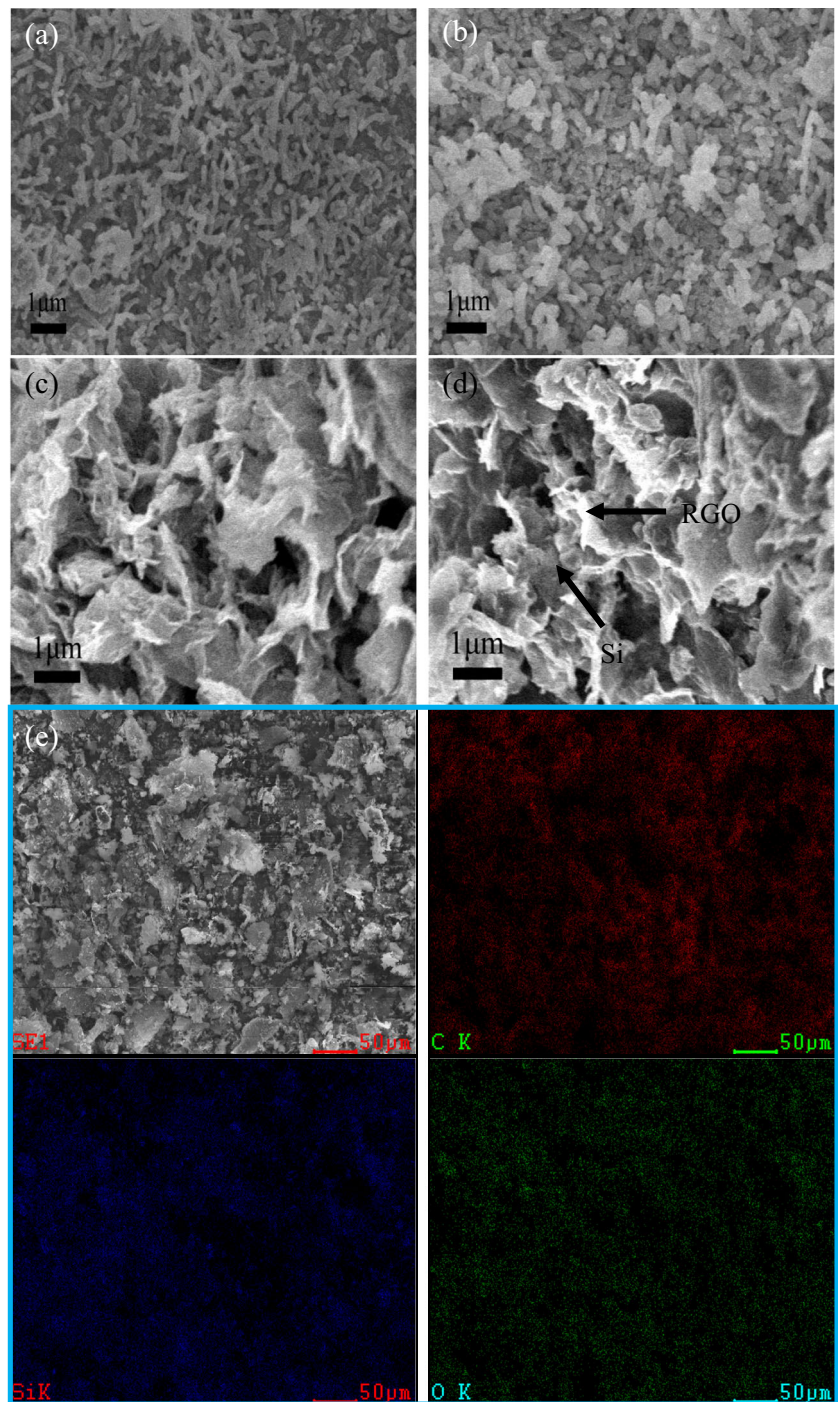
Fig. 1 X-ray diffraction patterns for graphite, graphite oxide, SBA-15, porous Si, and RGO/PS composite

a peak appears at about 10.5° corresponding to (001) plane, and the peak at 26.5° for graphite disappears, indicating the successful oxidation of graphite to graphite oxide [28]. In the case of SBA-15, a broad peak appears at around 24° , indicating that the synthesized SiO_2 is amorphous. After magnesiothermic reduction of SBA-15, the PS particles present well-defined peaks at 28.5° , 47.4° , 56.2° , 69.3° , 76.4° , and 88.2° , which are assigned to the (111), (220), (311), (400), (331), and (422) planes of crystallized Si, respectively. This

result suggests that the SiO_2 can be reduced successfully to Si by magnesiothermic reduction. In the case of RGO/PS composite, the peak at about 26.5° is corresponding to (002) plane of graphite, and other peaks are identical with those of PS, indicating the presence of both RGO and Si.

The morphologies of SBA-15, PS, graphene oxide, and RGO/PS composite were examined by FE-SEM, as shown in Fig. 2. SBA-15 is a rod-like structure with an average diameter about 100 nm and the average length about 1 μm (Fig. 2a).

Fig. 2 FE-SEM images of SBA-15 (a), porous Si (b), graphene oxide nanosheets (c), and RGO/PS composite (d) and FE-SEM image of RGO/PS composite and the corresponding elemental C, Si, and O EDS maps (e)



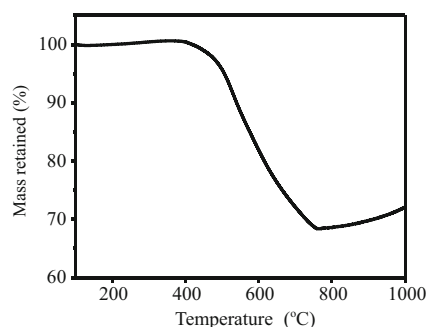


Fig. 3 TGA curve of RGO/PS composite under air atmosphere

After magnesiothermic reduction of SBA-15, the PS particles retain a rod-like structure and the average length decreases to

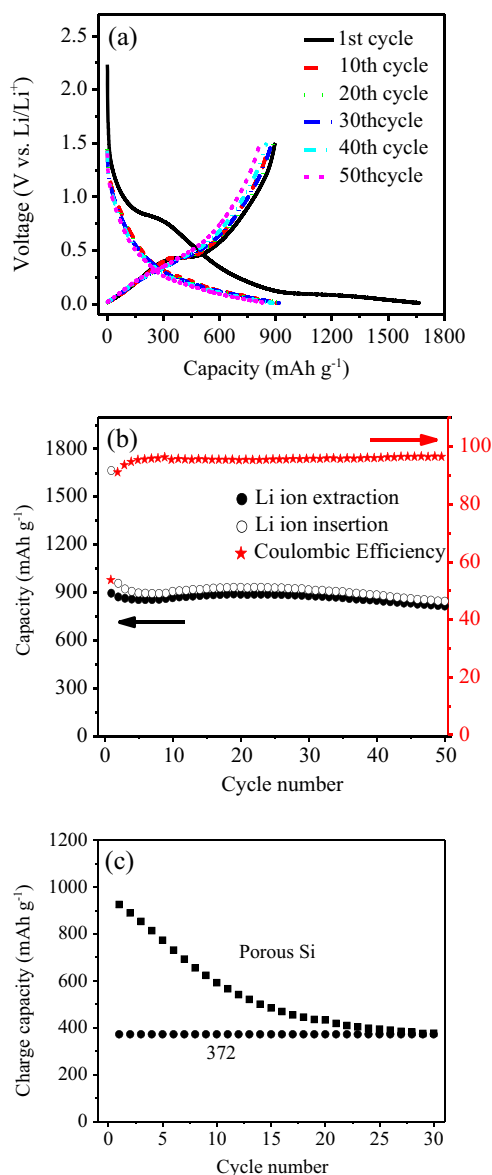


Fig. 4 The discharge–charge curves of RGO/PS composite cycled between 0.01 and 1.5 V at a rate of 100 mA g^{-1} (a). Cycling stabilities of RGO/PS composite (b) and porous Si (c) at a rate of 100 mA g^{-1} in the voltage range of 0.01–1.5 V

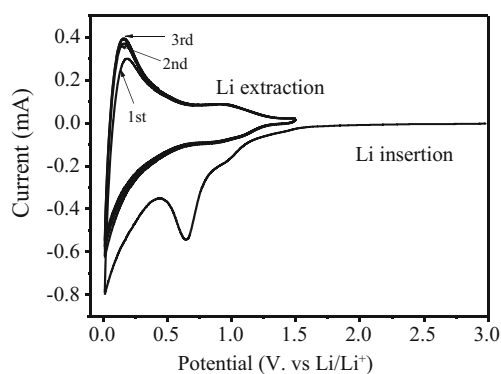


Fig. 5 Cyclic voltammetry of RGO/PS composite from 0.01 to 1.5 V vs. Li/Li^+ at a scan rate of 0.5 mV s^{-1}

about $0.5 \mu\text{m}$ (Fig. 2b). This may be due to that the part structure was destroyed during the magnesiothermic reduction process. The graphene oxide is a typical lamellar structure, and these nanosheets curl with each other (Fig. 2c). For the RGO/PS composite, the PS particles are fully and uniformly covered by RGO, and the morphology of rod-like PS may be destroyed partly during the synthesis process of RGO/PS (Fig. 2d). This structure avoids the direct contact between Si particles and electrolyte during discharge–charge process. The distribution of Si on the graphene could also be further confirmed from FE-SEM image with corresponding C, Si, and O maps using the characteristic X-ray spectroscopy (Fig. 2e), suggesting the uniform distribution of Si on graphene and the existence of residual SiO_2 in the composite.

To quantify the carbon and silicon contents in the composite, TGA was performed under air atmosphere. It can be estimated that the carbon and silicon weight contents are about 30 and 70 % from the TGA curve (Fig. 3), respectively. Figure 4a shows the discharge (lithium ion insertion) and charge (lithium ion extraction) profiles of RGO/PS composite for the first, 10th, 20th, 30th, 40th, and 50th cycles tested at a rate of 100 mA g^{-1} . In the case of RGO/PS composite electrode, it can be seen that the electrode exhibits two wide

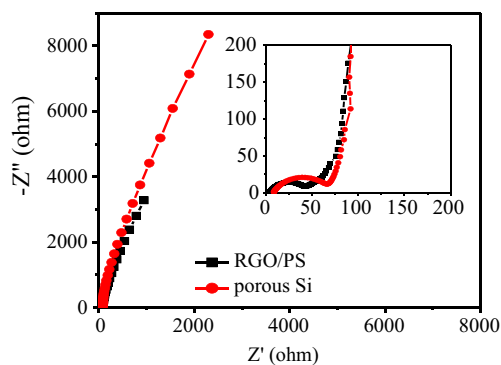


Fig. 6 Nyquist plots of RGO/PS composite and porous Si in an open-circuit potential. Magnified Nyquist plots (*inset*)

voltage plateaus at about 0.7 and 0.1 V during the first discharge process, which is attributed to the formation of SEI layer and Li_xSi alloy, respectively. The initial discharge and charge capacities are 1,665 and 895 mAh g^{-1} , respectively. The low initial discharge/charge capacities of RGO/PS composite may be due to the presence of residual SiO_2 in the composite. The large initial irreversible capacity may be caused by the decomposition of the electrolyte and the formation of SEI layer on the surface of electrode material [29, 30]. During the 10th cycle, the reversible capacity of 866 mAh g^{-1} is obtained and the corresponding coulombic efficiency is 95.5 %. Figure 4b shows the discharge/charge specific capacities and cycling stability of RGO/PS electrode. The reversible specific capacity of RGO/PS composite is about 815 mAh g^{-1} with a coulombic efficiency of 96.4 % during the 50th cycle under a current density of 100 mA g^{-1} . The discharge specific capacity and cycling stability of PS have been reported in our related work [11]. In contrast, the discharge capacity of PS electrode degrades rapidly to 376 mAh g^{-1} after 30 cycles, which is less than 1/2 times than that of the RGO/PS electrode after 50 cycles (Fig. 4c). The excellent cycling stability of RGO/PS composite is attributed to the fact that the RGO in the composite improves the electronic conductivity of electrode. Another reason for the enhanced performance could be due to that the RGO enhances the compatibility of electrode and electrolyte as a result of forming a stable SEI layer on the surface of electrode [31]. In addition, the good mechanical stability of RGO could effectively buffer the stress induced by volume variation of electrode materials during lithium ion insertion/extraction process. Moreover, the porous structure can accommodate the large volume changes during the discharge–charge process.

The CV curves measured at a scan rate of 0.5 mV s^{-1} over a voltage range from 0.01 to 1.5 V are shown in Fig. 5. There is a strong peak at 0.66 V during the first lithium insertion process, which disappears from the second cycles. This cathodic peak corresponds to the formation of SEI layer on the surface of electrode. The peak at 0.1 V is ascribed to the formation of Li_xSi alloy, which is consistent with the first discharge curve. For the anodic scans, the peaks at 0.23 V should correspond to the extraction of lithium ions from Li_xSi alloy electrode.

To further investigate the improved electrochemical performance, the Nyquist plots of PS and RGO/PS composite are compared in Fig. 6. Both the electrodes display one depressed semicircle in the high frequency and an inclined line in the low-frequency region. The high-frequency semicircles related to the overlap of SEI resistance and charge-transfer resistance are 73 and 48 Ω for the PS and RGO/PS, respectively. The results indicate that the RGO in the composite can improve the electronic conductivity and make for the formation of stable SEI layer on the surface of electrode.

Conclusion

The RGO/PS composite as anode materials for lithium ion batteries was prepared to accommodate the large volume changes of Si, and it exhibits a high reversible capacity of about 815 mAh g^{-1} after 50 cycles at a rate of 100 mA g^{-1} . The obtained excellent electrochemical properties of the fabricated RGO/PS composite electrode are attributed to combining the advantages of silicon (high capacity) with RGO (high electronic conductivity and excellent cycling stability). In addition, the RGO is beneficial to the formation a stable SEI layer on the surface of Si-based electrodes and offers a continuous electrically conductive network. The porous structure of RGO/PS composite facilitates the penetration of electrolyte and can accommodate the large volume changes.

Acknowledgments This work was supported by the Natural Science Foundation of China (NSFC, 51272128, 51302152, 51302153) and Excellent Youth Foundation of Hubei Scientific Committee (2011CDA093). Moreover, the authors are grateful to Dr. Jianlin Li at China Three Gorges University for his kind support to our research.

References

1. Winter M, Besenhard JO, Spahr ME, Novak P (1998) Insertion electrode materials for rechargeable lithium batteries. *Adv Mater* 10:725–763
2. Boukamp BA, Lesh GC, Huggins RA (1981) All-solid lithium electrodes with mixed-conductor matrix. *J Electrochem Soc* 128: 725–729
3. Li H, Huang XJ, Chen LQ, Wu ZG, Liang Y (1999) A high capacity nano-Si composite anode material for lithium rechargeable batteries. *Electrochem Solid State Lett* 2:547–549
4. Kim HJ, Seo M, Park MH, Cho J (2010) A critical size of silicon nano-anodes for lithium rechargeable batteries. *Angew Chem Int Ed* 49:2146–2149
5. Chan CK, Peng HL, Liu G, McIlwrath K, Zhang XF, Huggins RA, Cui Y (2008) High-performance lithium battery anodes using silicon nanowires. *Nat Nanotechnol* 3:31–35
6. Park MH, Kim MG, Joo J, Kim K, Ahn S, Cui Y (2009) Silicon nanotube battery anodes. *Nano Lett* 9:3844–3847
7. Magasinski A, Dixon P, Hertzberg B, Kvit A, Ayala J, Yushin G (2010) High-performance lithium-ion anodes using a hierarchical bottom-up approach. *Nat Mater* 9:353–358
8. Kim H, Cho J (2008) Superior lithium electroactive mesoporous Si@carbon core-shell nanowires for lithium battery anode material. *Nano Lett* 8:3688–3691
9. Cui LF, Yang Y, Hsu CM, Cui Y (2009) Carbon-silicon core-shell nanowires as high capacity electrode for lithium ion batteries. *Nano Lett* 9:3370–3374
10. Wang W, Kumta PN (2010) Nanostructured hybrid silicon/carbon nanotube heterostructures: reversible high-capacity lithium-ion anodes. *ACS Nano* 4:2233–2241
11. Tao HC, Fan LZ, Qu XH (2012) Facile synthesis of ordered porous Si@C nanorods as anode materials for Li-ion batteries. *Electrochim Acta* 71:194–200
12. Bolotin KI, Sikes KJ, Jiang Z, Klima M, Fudenberg G, Hone J, Kim P, Stormer HL (2008) Ultrahigh electron mobility in suspended graphene. *Solid State Commun* 146:351–355

13. Lee C, Wei XD, Kysar JW, Hone J (2008) Measurement of the elastic properties and intrinsic strength of monolayer graphene. *Science* 321: 385–388
14. Peigney A, Laurent C, Laurent E, Bacsa RR, Rousset A (2001) Specific surface area of carbon nanotubes and bundles of carbon nanotubes. *Carbon* 39:507–514
15. Wang GX, Shen XP, Yao J, Park J (2009) Graphene nanosheets for enhanced lithium storage in lithium ion batteries. *Carbon* 47: 2049–2053
16. Tao HC, Fan LZ, Yan XQ, Qu XH (2012) In situ synthesis of TiO₂-graphene nanosheets composites as anode materials for high-power lithium ion batteries. *Electrochim Acta* 69:328–333
17. Zhou GM, Wang DW, Li F, Zhang LL, Li N, Wu ZS, Wen L, Lu GQ, Cheng HM (2010) Graphene-wrapped Fe₃O₄ anode material with improved reversible capacity and cyclic stability for lithium ion batteries. *Chem Mater* 22:5306–5313
18. Chen SQ, Wang Y (2010) Microwave-assisted synthesis of a Co₃O₄-graphene sheet-on-sheet nanocomposite as a superior anode material for Li-ion batteries. *J Mater Chem* 20:9735–9739
19. Wang GX, Wang B, Wang XL, Park J, Dou SX, Ahnb H, Kim K (2009) Sn/graphene nanocomposite with 3D architecture for enhanced reversible lithium storage in lithium ion batteries. *J Mater Chem* 19:8378–8384
20. Wang ZY, Zhang H, Li N, Shi ZJ, Gu ZN, Cao GP (2010) Laterally confined graphene nanosheets and graphene/SnO₂ composites as high-rate anode materials for lithium-ion batteries. *Nano Res* 3: 748–756
21. Lee JK, Smith KB, Hayner CM, Kung HH (2010) Silicon nanoparticles-graphene paper composites for Li ion battery anodes. *Chem Commun* 46:2025–2027
22. Tao HC, Fan LZ, Mei YF, Qu XH (2011) Self-supporting Si/reduced graphene oxide nanocomposite films as anode for lithium ion batteries. *Electrochem Commun* 13:1332–1335
23. Chou SL, Wang JZ, Choucair M, Liu HK, Stride JA, Dou SX (2010) Enhanced reversible lithium storage in a nanosize silicon/graphene composite. *Electrochem Commun* 12:303–306
24. Kim H, Han B, Choo J, Cho J (2008) Three-dimensional porous silicon particles for use in high-performance lithium secondary batteries. *Angew Chem Int Ed* 47:10151–10154
25. Yu Y, Gu L, Zhu CB, Tsukimoto S, van Aken PA, Maier J (2010) Reversible storage of lithium in silver-coated three-dimensional macroporous silicon. *Adv Mater* 22:2247–2250
26. Hummers WS, Offeman RE (1958) Preparation of graphitic oxide. *J Am Chem Soc* 80:1339
27. Zhao DY, Feng JF, Huo QS, Melosh N, Fredrichson GH, Chemka BF, Strucky GD (1998) Triblock copolymer syntheses of mesoporous silica with periodic 50 to 300 angstrom pores. *Science* 279:548–552
28. Zhang Y, Guo L, Wei S, He Y, Xia H, Chen Q, Sun H, Xiao FS (2010) Direct imprinting of microcircuits on graphene oxides film by femtosecond laser reduction. *NanoToday* 5:15–20
29. Liu Y, Hanai K, Yang J, Imanishi N, Hirano A, Takeda Y (2004) Silicon/carbon composites as anode materials for Li-ion batteries. *Electrochem Solid-State Lett* 7:A369–A372
30. Kim I, Kumta PN, Blomgren GE (2000) Si/TiN nanocomposites novel anode materials for Li-ion batteries. *Electrochem Solid-State Lett* 3:493–496
31. Wu H, Chan G, Choi JW, Ryu I, Yao Y, McDowell MT, Lee SW, Jackson A, Yang Y, Hu L, Cui Y (2012) Stable cycling of double-walled silicon nanotube battery anodes through solid-electrolyte interphase control. *Nat Nanotechnol* 7:310–315